ACS Energy LETTERS

http://pubs.acs.org/journal/aelccp

# Ultrathin Light-Emitting Diodes with External Efficiency over 26% Based on Resurfaced Perovskite Nanocrystals

Qun Wan,[§] Weilin Zheng,[§] Chen Zou,[§] Francesco Carulli, Congyang Zhang, Haili Song, Mingming Liu, Qinggang Zhang, Lih Y. Lin, Long Kong, Liang Li,* and Sergio Brovelli*

Cite This: *ACS Energy Lett.* 2023, 8, 927−934

Read Online

ACCESS | Metrics & More | Article Recommendations | Supporting Information

**ABSTRACT:** **Light-emitting diodes based on perovskite nanocrystals (PNCs-LEDs) have gained great interest for next-generation display and lighting technologies prized for their color purity, high brightness, and luminous efficiency which approach the intrinsic limit imposed by light extraction from the device structure. Although the time is ripe for the development of effective light outcoupling strategies to further boost the device performance, this technologically relevant aspect of PNC-LEDs is still without a definitive solution. Here, following theoretical guidelines and without the integration of complex photonic structures, we realize stable PNC-LEDs with external quantum efficiency (EQE) as high as 26.7%. Key to such performance is channeling the recombination zone in PNC emissive layers as thin as 10 nm, which we achieve by finely balancing charge transport using $CsPbBr_3$ PNCs resurfaced with a nickel oxide layer. The ultrathin approach is general and, in principle, applicable to other perovskite nanostructures for fabricating highly efficient, color-tunable transparent LEDs.**

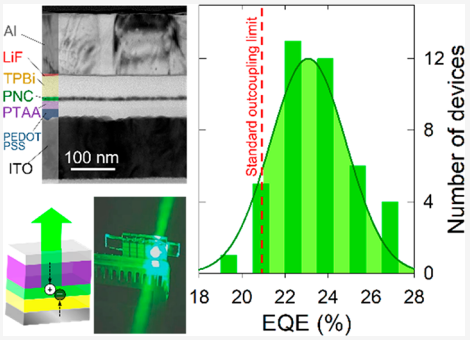


In the past few years, prized for their advantageous optical properties and affordable solution processability, lead halide perovskite nanocrystals (PNCs) have emerged as promising active materials in a wide range of photonic and optoelectronic technologies, spanning from photovoltaic cells,[1−5] lasers,[6,7] data communication,[8] and radiation detectors[9−11] to luminescent solar concentrators[12,13] and artificial light sources.[14−25] Light-emitting diodes based on PNCs (PNC-LEDs)[26−32] have experienced a particularly steep growth,[33,34] owing to the efficient, spectrally tunable, narrow luminescence of PNCs and their defect-tolerant electronic structure.[27,35−41] Building upon these unique qualities of PNCs, extensive research in material design, morphology/interfacial control,[42] surface chemistry,[15,17,27,30,37−39,43−49] and energy level engineering (via doping or alloying)[38,50,51] has been dedicated to understanding and suppressing detrimental surface defects—acting both as traps for electrically injected carriers and as nonradiative quenching centers for the resulting excitonic luminescence—and to devise suitable molecular ligands and solution-based protocols for fabricating high-quality, low-resistance PNC active layers.[17,20,36,37,47,52−54] These efforts have enabled researchers to incorporate PNCs with ∼100% photoluminescence (PL) quantum yield ($\Phi_{PL}$) in devices featuring near-unity carrier mobility ratio ($\gamma$),[55] resulting in internal quantum efficiency (IQE = $\gamma \times \eta_{S/T} \times \Phi_{PL}$, corresponding to the ratio between the number of photons emitted from the active region and the number of electrons injected into the LED) close to 100% ($\eta_{S/T}$ is the singlet to triplet ratio that, in halide perovskite materials, is close to one[56]). As a result, external quantum efficiency (EQE = IQE × $\eta_{OC}$, corresponding to the ratio between the number of photons emitted to free space and the number of electrons injected into the LED) of 21.6% was obtained by Chiba et al.[26] using red-emitting $CsPb(Br/I)_3$, and EQE = 23.4% was recently reported by Kim et al.[45] using cation alloyed PNCs with emission in the green region, in either case matching the record performance of analogous LEDs based on perovskite thin films.[28,57,58] One key aspect of the best perovskite LED devices (PNC- or thin-film-based) reported to date is their particularly high light extraction efficiency from the device structure, $\eta_{OC}$, which is determined by the refractive index, absorbance, thickness, and structure of the device layers.[59−64]

**Received:** December 9, 2022
**Accepted:** December 28, 2022
**Published:** January 10, 2023

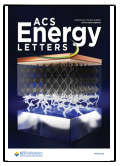

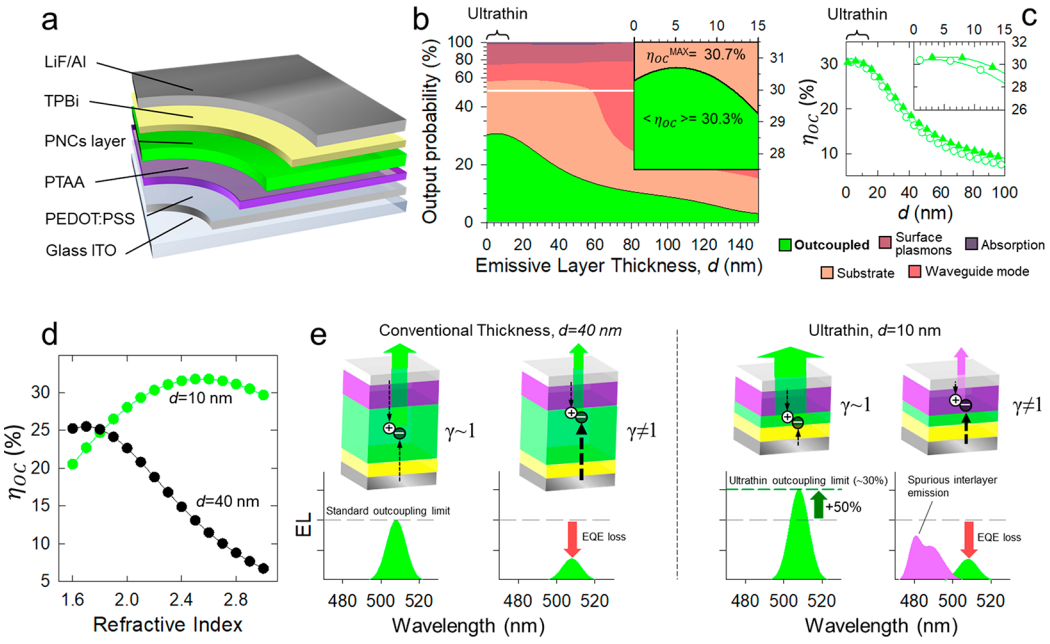


**Figure 1.** (a) Schematic depiction of a PNC-LED with the architecture used for the light outcoupling simulation. (b) Outcoupling probability distribution as a function of the thickness of the emissive layer, *d*, for a PNC-LED with the same structure as in panel a. The output probability depends strongly on the refractive index and thickness of all functional layers; therefore, particular care is suggested when comparing the simulated data with literature reports. (c) Comparison between $\eta_{OC}$-values vs *d* computed by considering (triangles) or excluding (circles) photon recycling effects. (d) $\eta_{OC}$ as a function of the refractive index of ultrathin ($d$ = 10 nm, green circle) and standard ($d$ = 40 nm, black circles) active layer thickness. (e) Illustration of the effect of the positioning of the carrier recombination zone in balanced ($\gamma = 1$) vs unbalanced ($\gamma \neq 1$) LEDs with standard or ultrathin active layers. For standard thickness devices, small charge imbalance lowers the efficiency, but the recombination zone is maintained within the PNC active layer, thus preserving the color purity of the EL. In unbalanced ultrathin LEDs, exciton formation and decay occur mostly in the charge-regulating layer (the HTL in the depicted case) leading to severe parasitic emission (in purple) in addition to efficiency losses.

To highlight the role of $\eta_{OC}$ in the EQE, it is instructive to theoretically simulate the maximum achievable performance (considering IQE = 100%) of a planar device with the commonly employed architecture shown in Figure 1a as a function of the thickness of a $CsPbBr_3$ PNC emissive layer (indicated as *d*). In our calculations, we considered the same device architecture employed to realize the ultrathin LEDs reported later in this work, featuring an indium tin oxide (ITO) coated (thickness 150 nm) glass anode coated with poly(3,4-ethylenedioxythiophene):polystyrene (PEDOT:PSS, 20 nm)/Poly(bis(4-phenyl)(2,4,6-trimethylphenyl)amine) (PTAA, 20 nm) hole injection/transport layers and 2,2′,2″-(1,3,5-benzinetriyl)-tris (1-phenyl-1-H-benzimidazole) (TPBi) (45 nm) electron transport layer covered with a LiF/Al (1 and 100 nm respectively) cathode. For the refractive index of the $CsPbBr_3$ PNC emissive layer, we employed $n$ = 2.18, as measured by ellipsometry (Supporting Figure S1). Photon recycling effects caused by multiple reabsorption and re-emission events of the electroluminescence (EL) were taken into account following the approach described in refs 65 and 66. In order to emphasize the effect solely of *d* without additional contributions from, for example, light scattering due to rough surface/interface morphology that artificially enhances light outcoupling, all layers were assumed as perfectly flat, also consistent with the very smooth film morphology of our real devices (*vide infra*). Consistent with previous reports, the simulation in Figure 1b shows that for $d$ = 35−60 nm, the maximum achievable EQE reaches ∼21−22%, whereas the majority of the EL is lost due to the high refractive index of the perovskite material, parasitic contributions by the substrate, waveguiding modes, surface plasmons, and light absorption of the interlayers.

For this reason, effective outcoupling strategies for the extraction of internal light are extremely powerful and highly sought-after for progressing PNC LED performances beyond the state-of-the-art. Several approaches have been successfully applied to organic or quantum dot-based LEDs,[61,67−74] including the engineering of the refractive index, orientation of the emitter's dipole, the integration of photonic structures (i.e., microlense arrays, diffraction gratings, low-index grids, or buckling patterns inside the LED) or the optimization of the thickness of the charge-regulating layers so as to exploit microcavity effects. The use of patterned substrates or the spontaneous formation of submicrometer structures[16] have been found helpful for enhancing light outcoupling from organometallic perovskite LEDs.[27,74] Very recently, Kumar et al. exploited anisotropic emission from PNC superlattices to obtain peak EQE as high as 23.94% (average value ⟨EQE⟩ = 17.89%)[75] and Ciu et al.[76] used aligned perovskite nanoplatelets to obtain a light-outcoupling efficiency of ∼31%, substantially higher than that of isotropic emitters (∼23%), although the LED efficiency remained lower than 5%.

An alternative approach to enhanced light extraction emerging from the theoretical simulation is thinning the emissive layer to $d \approx 10$ nm (indicated here as the *ultrathin regime*, Figure 1b). This should decrease the effective refractive index of the functional layers, substantially reducing the fraction of light trapped in waveguiding modes, ultimately enabling one to boost the EQE to over ∼30% without the need for complex photonic components (corresponding to ca. 50% enhancement


https://doi.org/10.1021/acsenergylett.2c02802
ACS Energy Lett. 2023, 8, 927−934

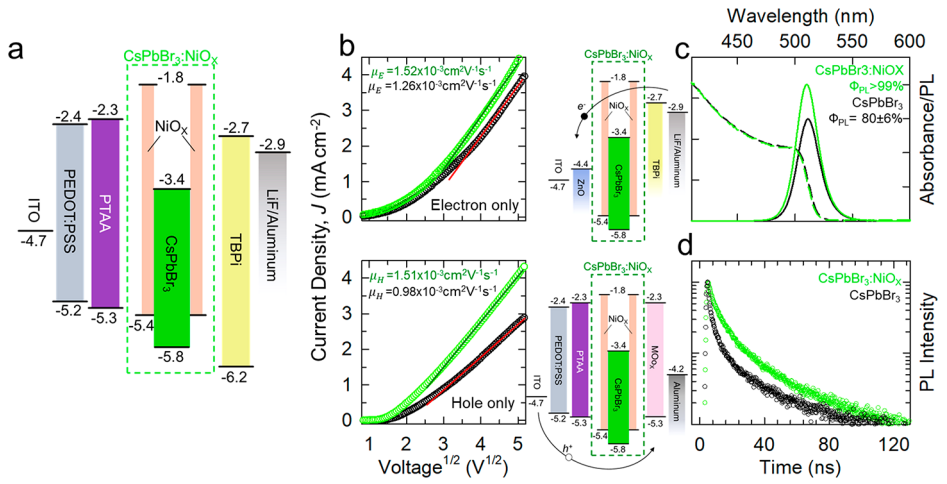


**Figure 2. (a) Flat band energy diagram of a multilayer LED highlighting the shift of the frontiers level of $CsPbBr_3$ PNCs upon treatment with $NiO_X$. (b) Carrier mobility (top panel, electrons; lower panel, holes) in single carrier devices embedding pristine $CsPbBr_3$ PNCs (black symbols) or $CsPbBr_3$:$NiO_X$ PNCs (green symbols). (c) Optical absorption (dashed lines) and PL (solid lines) spectra of pristine (black) and $NiO_X$-treated $CsPbBr_3$ PNCs (green) in toluene solution (excitation at 450 nm) and (d) respective PL decay curves.**

with respect to standard thickness conditions). Consistent with previous results,[65,66] for ultrathin LEDs, photon recycling plays a minor role in the outcoupling probability (~2% for 10 nm thin devices, Figure 1c and Supporting Figure S2); however, due to the substantial overlap between the absorption and emission profiles and the near-unity $\Phi_{PL}$ of our PNCs, such processes become more relevant for devices embedding thicker emissive layers, leading to higher EQE values with respect to what is commonly predicted by neglecting photon recycling. Importantly, as shown in Figure 1d, in the ultrathin regime, $\eta_{OC}$ is found to slightly increase using emissive layers with high refractive index, in stark contrast to the substantial drop observed for thicker devices (i.e., $d$ = 40 nm vs $d$ = 10 nm). This is an additional valuable benefit of this motif, as it opens the possibility of exploring a wider range of materials with even higher refractive index than common halide perovskites (typically featuring $2.1 \leq n \leq 2.7$, depending on the halide composition, preparation method, etc.),[77,78] without sacrificing—and possibly further enhancing—the maximum achievable LED efficiency. Finally, the realization of ultrathin PNC-LEDs would prompt their applicability to special situations where semitransparency is a mandatory prerequisite, such as unobtrusive LED displays and screens, augmented reality, and wearable technology.

However, despite the great potential of the approach, the practical realization of highly efficient LEDs with ultrathin PNC layers is extremely challenging, as it requires perfect equalization of the electron/hole currents inside the device, far beyond the operation conditions of common PNC-LEDs, and fine material processing to avoid the formation of pinholes in such a thin active layer. As sketched in Figure 1e, this is because small imbalances in charge injection/transport that are bearable for larger $d$ values—although still lowering the EQE—in the ultrathin regime have the additional damaging effect of locating the electron−hole recombination zone outside the emissive layer. This results in severe efficiency drop and in spurious parasitic EL from the organic charge-regulating layers, with consequent detriment of the LED color purity, as demonstrated by control experiments reported later in this work. Finally, being made up of a small number of PNCs, ultrathin active films could be more affected by degradation (i.e., thermal, electrical, etc.) than thick analogues, resulting in poor device stability. Therefore, in order to exploit the full potential of the ultrathin regime to overcome the outcoupling limit, specific material design strategies are strictly needed.

In this work we aim to contribute to this challenge by practically realizing highly reproducible, stable, color-pure, and bright ultrathin PNC-LEDs with EQE systematically exceeding the common outcoupling limit (⟨EQE⟩ = 23.1%, champion EQE as high as 26.7%) that, to the best of our knowledge, overcome any perovskite-based LEDs reported to date without additional photonic outcoupling components. To achieve this regime, we took inspiration from the substantial improvement of the hole mobility and device stability observed in organic and quantum dot LEDs[79−82] and perovskite solar cells featuring nickel oxides hole injecting layers[83−87] to devise a postsynthesis $NiO_X$ resurfacing treatment that synergistically optimizes all three key parameters that determine the EQE (namely $\gamma$, $\eta_{OC}$, and $\Phi_{PL}$). The application of this motif to both standard and advanced $CsPbBr_3$ PNCs, resulted in essentially perfectly equalized carrier injection and mobility that ultimately enabled us to focus the recombination zone into active layers as thin as $d$ = 10 nm—matching the low thickness limit set by the particle size—and to simultaneously enhance $\Phi_{PL}$ and device operational stability.

For our study, we employed state-of-the-art $CsPbBr_3$ PNCs synthesized using the triple ligand method,[88] as well as "control" PNCs of the same composition fabricated via a conventional hot injection route, that further generalize the ultrathin strategy for overcoming the outcoupling limit. In both cases, the PNCs were resurfaced with a hole-transporting $NiO_X$ layer using the multistep postsynthesis treatment described in detail in Materials and Methods in the Supporting Information. Based on the nearly identical effect on the structural and physical properties of PNCs produced through the two different synthetic approaches, we focus hereafter on PNCs obtained via the triple-ligand method that yields the best device performance via a more sustainable room-temperature route (the corresponding results on standard PNCs are reported in Figures S20−S26). The complete study of the effects of surface functionalization on the structure and composition of either PNC sample, including transmission electron microscopy


https://doi.org/10.1021/acsenergylett.2c02802
ACS Energy Lett. 2023, 8, 927−934

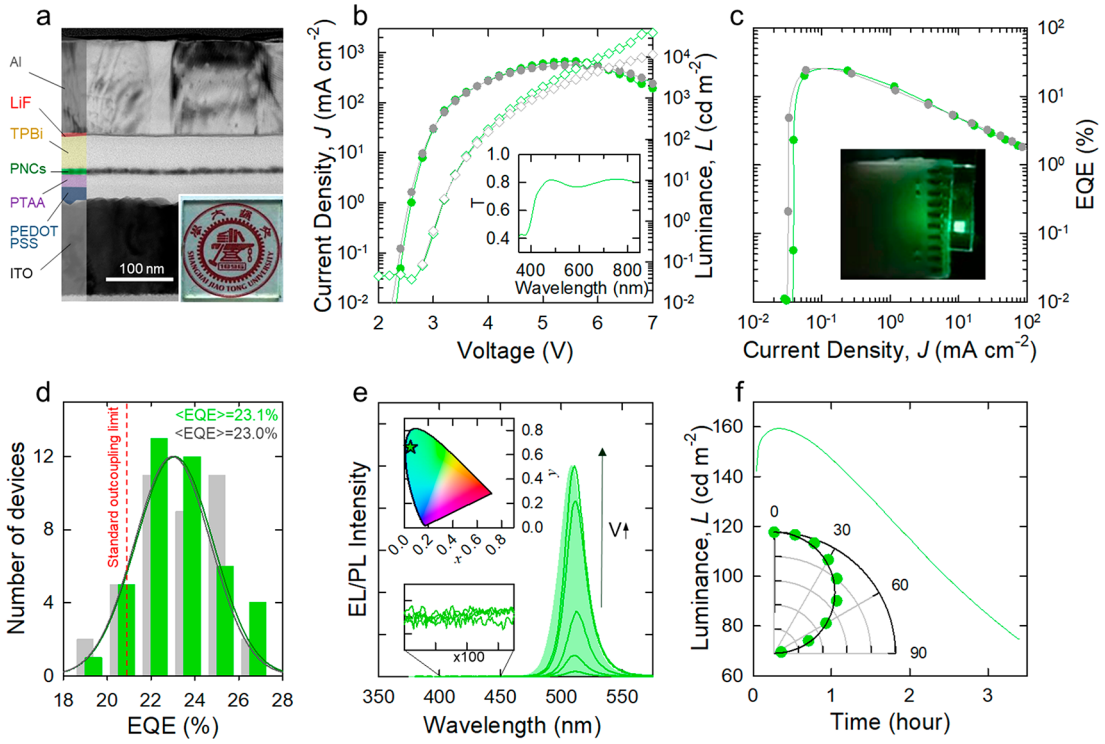


**Figure 3. (a) Cross-sectional TEM images of an LED sample embedding an ultrathin active layer of $CsPbBr_3$:$NiO_X$ PNCs. (b) Current density−voltage ($J$−$V$, hollow diamond) and voltage−luminance ($L$−$V$, full circles) characteristics of a representative $CsPbBr_3$:$NiO_X$ PNCs-based LED measured in our lab (green lines) and independently at the Research Center of Photoelectric Materials and Devices by the Department of Electronic Engineering of the Shanghai Jiao Tong University (gray lines). The characterization was performed at room temperature in air with simple device encapsulation. Inset: Transmission spectrum of the LED ($d$ = 10 nm) without the metal cathode. (c) EQE curves of the same LED reported in panel b (same color code as in panel b). Inset: photograph of a $CsPbBr_3$:$NiO_X$ PNCs-based LED (active area 4 $mm^2$). (d) EQE statistics over 40 identical ultrathin LEDs ($d$ = 10 nm) embedding $CsPbBr_3$:$NiO_X$ PNCs synthesized through a room-temperature approach (green bars) and hot injection method (gray bars). Bar width 1.5%. (e) EL spectra (dark green curves) of an ultrathin LED embedding $CsPbBr_3$:$NiO_X$ ($d$ = 10 nm) at increasing bias voltage (3−7 V as indicated by the arrow) together with the respective PL spectrum (shaded curve, excitation wavelength 450 nm). Bottom Inset: enlargement (×100) of the 380−470 nm region showing no emission by the organic interlayers. Top Inset: Chromaticity coordinates corresponding to the EL spectra of the ultrathin PNC-LED based on $CsPbBr_3$:$NiO_X$ shown in the CIE chromaticity diagram, highlighting the vicinity of the color coordinates to the spectral locus. (f) Luminance as a function of operating time of a representative $CsPbBr_3$:$NiO_X$ PNCs-based LED tested at room temperature in air with simple encapsulation. Inset: Angular emission profile of the same LED. The black line indicates the expected angular intensity distribution for a perfectly Lambertian emitter.**

(TEM) images, size distribution, X-ray diffraction patterns, and elemental mapping of pristine and $NiO_X$-treated $CsPbBr_3$ (hereafter refer to as $CsPbBr_3$:$NiO_X$) PNCs, is reported in Figures S3−S5. TEM images evidence no difference in particle shape or size before and after resurfacing (average size of 10.4 ± 1.5 and 11.5 ± 0.9 nm, respectively) in both cases showing cubic lattice (with a possible slight shift to the orthorhombic phase in the treated particles). The presence of nickel atoms adsorbed onto the particle surfaces as $NiO_X$ species was confirmed by the elemental analysis and the surface etching experiment combined with X-ray absorption spectroscopy measurements (XANES and EXAFS) shown in Figures S6 and S7. FTIR and NMR experiments shown in Figures S8 and S9 further reveal that following the $NiO_X$ treatment, most of the oleic acid and part of the oleylamine ligands are removed from the particle surfaces leaving mainly didodecyldimethylammonium bromide moieties.

Fundamentally, the $NiO_X$ layer has noticeable beneficial effects on the electrical and optical properties of the PNCs, which are both crucial for the realization of highly efficient ultrathin LEDs. Specifically, as shown by the flat-band energy diagram of pristine and $CsPbBr_3$:$NiO_X$ PNCs (Figure 2a) and by ultraviolet photoelectron spectroscopy (UPS) measurements reported in Figure S10, the treatment produces a $NiO_X$ coating featuring an ∼400 meV offset with respect to both frontier levels of $CsPbBr_3$ PNCs. This introduces an intermediate energy step at −5.4 eV between the HOMO level of PTAA ($E_{HOMO}$ = −5.25 eV) and the valence band of the PNCs ($E_{VB}$ = −5.8 eV), which substantially facilitates hole injection. The effect on electron injection is negligible due to the already favorable potential offset between the LUMO of TPBi and the PNC conduction band and the very low thickness of the dielectric barrier constituted by the $NiO_X$ layer. Importantly and in agreement with previous studies on organic and quantum dot LEDs using nickel oxides interlayers to enhance hole injection and transport,[79−81] carrier mobility measurements by a space-charge limited current (SCLC) method in single carrier devices (Figure 2b) show that the hole mobility increases from the typical value[26,89] of $\mu_h = 0.98 \pm 0.10 \times 10^{-3}$ $cm^2\ V^{-1}\ s^{-1}$ to $\mu_h = 1.51 \pm 0.18 \times 10^{-3}$ $cm^2\ V^{-1}\ s^{-1}$ upon $NiO_X$ resurfacing, closely matching the respective electron mobility, which also grows from $\mu_e = 1.26 \pm 0.18 \times 10^{-3}$ $cm^2\ V^{-1}\ s^{-1}$ to $\mu_e = 1.52 \pm 0.16 \times 10^{-3}$ $cm^2\ V^{-1}\ s^{-1}$. Altogether, this results in essentially perfect carrier mobility balance in devices based on $CsPbBr_3$:$NiO_X$ PNCs, as quantified by the term $\gamma = \mu_e/\mu_h$ that approaches unity ($\gamma$ = 1.08 ± 0.07) with respect to the pristine case featuring $\gamma$ = 1.29 ± 0.06. Due of the initially lower mobilities in conventional


https://doi.org/10.1021/acsenergylett.2c02802
ACS Energy Lett. 2023, 8, 927−934

PNC solids, the mobility balance increases even more substantially after $NiO_X$ treatment for the standard $CsPbBr_3$ PNCs, with $\gamma$ changing from 1.50 ± 0.04 in the pristine case to $\gamma$ = 1.09 ± 0.08. We notice that this effect is also likely corroborated by the PNC washing process and by the effective passivation of surface carrier traps posited by $NiO_X$. Suppression of surface trapping is confirmed by the side-by-side spectroscopic analysis shown in Figure 2c,d. Upon $NiO_X$ resurfacing, the PL quantum yield grows from $\Phi_{PL}$ = 80 ± 6% of the pristine PNCs to $\Phi_{PL}$ > 99% ($\Phi_{PL}$ = 48 ± 6% to 95 ± 6% for the standard PNCs), accompanied by a noticeable lengthening of the decay kinetics. We highlight that the spectral position of the first excitonic absorption and luminescence peaks are essentially identical in the reference and $CsPbBr_3$:$NiO_X$ PNCs samples, indicating that the electronic structure of the nanocrystal's core is unaltered by the treatment, and that the bands alignment at the heterointerface does not cause exciton splitting, which is consistent with ∼1 monolayer thin $NiO_X$ coating. We finally notice that the PL spectrum of $NiO_X$-treated PNCs is slightly blue-shifted with respect to the pristine PNCs, which is likely the consequence of the effective passivation of surface defect sites (likely halide vacancies) in agreement with recent literature.[11,90]

We then proceeded with experimentally validating the potential of the ultrathin emissive layer approach by fabricating and testing planar devices with the architecture shown in Figure 1a embedding an ultrathin PNC emissive layer ($d$ = 10 nm). The cross-sectional TEM image is reported in Figure 3a, showing a continuous film of $CsPbBr_3$:$NiO_X$ PNCs with clear interfaces. The surface morphology of the interlayers and of the ultrathin PNC film deposited onto ITO/PEDOT:PSS/PTAA was investigated by atomic force microscopy revealing uniform, continuous films with RMS roughness as low as 0.63 and 2.04 nm, respectively (Figure S11). As anticipated above, the smoothness of the interfaces is important for our discussion as it minimizes light-scattering effects on light outcoupling, consistent with the simulations in Figure 1b. The whole device shows an ultralow thickness of about 400 nm (excluding the glass substrate) resulting in substantial transparency across the visible spectrum, as shown by the photograph of the complete device, except for the metal cathode, reported in the inset of Figure 3a and by the corresponding transmission spectrum in the inset of Figure 3b. Consistently, the color rendering index of transmitted light from D65 standard illuminant[91] is as high as $R_a$ = 95. Although the engineering of fully transparent LEDs including the cathode material is beyond the scope of this study, Supporting Video 1 shows an example of a functioning ultrathin LED with a semitransparent cathode (20 nm) emitting light from both sides.

In Figure 3b,c we report the current density−voltage ($J$−$V$) and luminance−voltage ($L$−$V$) responses of a representative LED embedding an ultrathin layer of $CsPbBr_3$:$NiO_X$ PNCs ($d$ = 10 nm). The LED shows low turn on voltage ($V_{ON}$, defined as the voltage at which the luminance is 1 cd/m$^2$) of 2.8 V, high luminance up to ∼5000 cd/m$^2$ and EQE = 23.7%, which substantially exceeds the outcoupling limit of conventional devices. External confirmation of the result was provided by independent measurements on the same device. The repeatability of our result over 40 identical devices (featuring $d$ = 10 nm, complete statistics are reported in Table S3) is highlighted in Figure 3d showing that nearly all produced LEDs exceeded the outcoupling limit for standard PNC-LEDs and thus systematically outcompeted any perovskite-based LEDs with emission in any spectral region reported to date, with average ⟨EQE⟩ = 23.1 ± 1.7% and champion $EQE_C$ = 26.7%. The statistics over the same number of devices produced using conventional $CsPbBr_3$ PNCs resurfaced with $NiO_X$ are also reported showing, also in this case, very high EQE systematically exceeding the outcoupling limit ($EQE_C$ = 26.6%, ⟨EQE⟩ = 23.0 ± 1.7%, complete statistics are reported in Table S4), consistent with the near-unity $\Phi_{PL}$ registered also for such PNCs. We highlight that our statistics include devices embedding PNCs from different synthesis batches, further corroborating the repeatability of the approach. Crucially, at any driving voltage (up to 7 V), the EL spectrum features exclusively a narrow (fwhm = 20 nm) peak at 514 nm (Figure 3e), matching the respective PL profile. The corresponding Commission Internationale de l'Eclairage coordinates are $x$ = 0.05 and $y$ = 0.66, corresponding to ∼90% saturated green light. No spurious emission from the organic interlayers is observed, which confirms that the recombination zone is fully confined in the ultrathin active layer and that the emissive layer is a continuous film of PNCs even at such a low thickness level. Devices with gradually increasing $d$ showed progressively higher $V_{ON}$ from 2.8 V to 5.2 V accompanied by the drop of the luminance and EQE below the respective maximum theoretical value, which indicates that the IQE decreases in thicker PNC films, likely due to electrical losses in thicker PNC layers, which are not taken into account in the optical simulation (Table S1).

More importantly, despite their very low thickness, our LEDs with an ultrathin active layer exhibited constant electrical luminescent response fully preserved for several consecutive voltage scans (Figure S12) and operational luminance stability comparable to the best devices reported to date featuring much thicker emissive films, with half-lifetime ($T_{50}$, defined as the time after which the luminance decreases by a factor of 2) as long as $T_{50}$ = 3 h when operated at constant current density of 1 mA/cm$^2$ (corresponding to initial luminance $L_0$ ≈ 150 cd m$^{-2}$ (Figure 3f)) and $T_{50}$ = 15 min when driven at 8 mA/cm$^2$ corresponding to $L_0$ = 1200 cd m$^{-2}$ (Figure S13). Such stability is likely due to the combined beneficial effect of the triple-ligand approach used for the PNC synthesis and to the $NiO_X$ resurfacing, as supported by the substantially lower stability of comparable LEDs embedding pristine $CsPbBr_3$ NCs (Figure S14) and in agreement with recent reports on stable perovskite solar cells with nickel oxide interlayers.[84,85] Finally, angular resolved electroluminescence measurements of our ultrathin LED featuring a $CsPbBr_3$:$NiO_x$ PNCs active layer showed Lambertian emission distribution (inset of Figure 3f), thus indicating that exceeding the outcoupling limit is not due to microcavity effects,[47] in agreement with our theoretical prediction. We emphasize that ultrathin LEDs with the performance shown in Figure 3 cannot be achieved with simple pristine $CsPbBr_3$ PNCs produced with either synthetic approach. As shown in Figure S15, already at conventional thicknesses ($d$ = 40 nm), control LEDs based on pristine PNCs exhibit only half the EQE and maximum luminance in comparison to analogue devices featuring $NiO_X$ treated particles. Furthermore, because of disproportionate charge injection and transport and of discontinuities in the film structure, the electroluminescence spectrum of a control LED with $d$ < 12 nm features a strong blue emission emerging from carrier recombination in the hole transport layer Figure S16. The whole characterization of the control devices is reported in Figure S17 and Table S2, showing, in agreement with previous results,[14,35] that the thinning approach also helps improve the efficiency of conventional PNC-LEDs that, however, feature


https://doi.org/10.1021/acsenergylett.2c02802
ACS Energy Lett. 2023, 8, 927−934

overall lower performance due to limited optical and electrical properties of standard $CsPbBr_3$ PNCs. We finally point out that also the amount of $NiO_X$ is crucial for maximizing the LED functioning as shown in Figures S18 and S19 and Table S5.

In conclusion, we have demonstrated that overcoating $CsPbBr_3$ PNCs with a layer of $NiO_X$ boosts the luminescence efficiency and equalizes the charge balance in LEDs, further enabling us to thin the active layer to 10 nm, which systematically enhances the efficiency of PNC-LEDs above the maximum value imposed by light outcoupling in standard devices, reaching EQE values exceeding 26%. The approach, demonstrated here using $CsPbBr_3$ PNCs produced via both room-temperature and hot injection methods is general and, in principle, applicable to other perovskite nanostructures for fabricating highly efficient, color-tunable LEDs. It is also compatible with the artificial introduction of outcoupling photonic structures for further boosting the device performance. These results offer a potentially powerful strategy for high-efficiency perovskite LEDs and a valuable route for next-generation display and lighting technologies.

## ■ ASSOCIATED CONTENT

### Supporting Information

The Supporting Information is available free of charge at https://pubs.acs.org/doi/10.1021/acsenergylett.2c02802.

Detailed description of PNC synthesis and experimental methods; structural and optical characterization of PNCs, such as PNC size distribution, XRD, elemental mapping $^1H$ NMR, characterization of LED morphology and performance, and outcoupling simulation (PDF)

Supporting Video 1: example of a functioning ultra-thin LED with a semitransparent cathode (20 nm) emitting light from both sides(MP4)

## ■ AUTHOR INFORMATION


### Corresponding Authors

**Liang Li** − *Macao Institute of Materials Science and Engineering (MIMSE), Macau University of Science and Technology, Taipa 999078 Macao, China;* orcid.org/0000-0003-3898-0641; Email: lli@must.edu.mo

**Sergio Brovelli** − *Dipartimento di Scienza dei Materiali, Università degli Studi di Milano-Bicocca, 20125 Milano, Italy;* orcid.org/0000-0002-5993-855X; Email: sergio.brovelli@unimib.it

### Authors

**Qun Wan** − *School of Environmental Science and Engineering, Shanghai Jiao Tong University, 200240 Shanghai, China*

**Weilin Zheng** − *School of Environmental Science and Engineering, Shanghai Jiao Tong University, 200240 Shanghai, China*

**Chen Zou** − *State Key Laboratory of Modern Optical Instrumentation, College of Optical Science and Engineering, Zhejiang University, Hangzhou 310058, China*

**Francesco Carulli** − *Dipartimento di Scienza dei Materiali, Università degli Studi di Milano-Bicocca, 20125 Milano, Italy;* orcid.org/0000-0002-8345-6606

**Congyang Zhang** − *Department of Electrical and Computer Engineering, University of Washington, Seattle, Washington 98195, United States*

**Haili Song** − *Key Laboratory of Bioinorganic and Synthetic Chemistry of Ministry of Education, School of Chemistry, Sun Yat-Sen University, Guangzhou 510275, China*

**Mingming Liu** − *School of Environmental Science and Engineering, Shanghai Jiao Tong University, 200240 Shanghai, China*

**Qinggang Zhang** − *School of Environmental Science and Engineering, Shanghai Jiao Tong University, 200240 Shanghai, China*

**Lih Y. Lin** − *Department of Electrical and Computer Engineering, University of Washington, Seattle, Washington 98195, United States;* orcid.org/0000-0001-9748-5478

**Long Kong** − *School of Environmental Science and Engineering, Shanghai Jiao Tong University, 200240 Shanghai, China*

Complete contact information is available at: https://pubs.acs.org/10.1021/acsenergylett.2c02802

### Author Contributions

§Q.W., W.Z., and C.Z. contributed equally to this work.


### Notes

The authors declare no competing financial interest.

## ■ ACKNOWLEDGMENTS

This work was supported by Joint Funds of the National Natural Science Foundation of China (No.U21A20320), the National Natural Science Foundation of China (NSFC 22175113) and "Pioneer" and "Leading Goose" R&D Program of Zhejiang (2022C03002). We gratefully acknowledge financial support from the Italian Ministry of University and Research (MIUR) through the grant Dipartimenti di Eccellenza-2017 "Materials for Energy". We want to give a special thanks to Professor Gufeng He in the Research Center of Photoelectric Materials and Devices for his help to confirm the performance of devices and Professor Baoquan Sun and Dr. Yatao Zou in Soochow University for their help in measuring the angular distribution of the emission pattern. We also thank the instrumental analysis center of Shanghai Jiao Tong University and the staff (Zhongqiu Bao, Ying Zhang, Yao Han, Chong Lu, Xinqiu Guo, and Jiaxin Ding) for help in SEM, TEM, and TOF SIMS measurements. Center for Advanced Electronic Materials and Devices of Shanghai Jiao Tong University supported the measurements of ellipsometry (Semilab SE-2000) and film thickness (KLA-Tencor P7). S.B. and F.C. acknowledge support from the Ministry of University and Research (MIUR) through grant "Dipartimenti di Eccellenza−2017 Materials For Energy". This work is dedicated to the heartfelt memory of our colleague and friend Gianluca Latini.

## ■ REFERENCES

(1) de Quilettes, D. W.; Vorpahl, S. M.; Stranks, S. D.; Nagaoka, H.; Eperon, G. E.; Ziffer, M. E.; Snaith, H. J.; Ginger, D. S. *Science* **2015**, *348* (6235), 683−686.

(2) Jeon, N. J.; Noh, J. H.; Yang, W. S.; Kim, Y. C.; Ryu, S.; Seo, J.; Seok, S. I. *Nature* **2015**, *517* (7535), 476.

(3) Kojima, A.; Teshima, K.; Shirai, Y.; Miyasaka, T. *J. Am. Chem. Soc.* **2009**, *131* (17), 6050−6051.

(4) Liu, M.; Johnston, M. B.; Snaith, H. J. *Nature* **2013**, *501* (7467), 395.

(5) Tsai, H.; Nie, W.; Blancon, J.-C.; Stoumpos, C. C.; Asadpour, R.; Harutyunyan, B.; Neukirch, A. J.; Verduzco, R.; Crochet, J. J.; Tretiak, S.; et al. *Nature* **2016**, *536* (7616), 312.

(6) Xing, G.; Mathews, N.; Lim, S. S.; Yantara, N.; Liu, X.; Sabba, D.; Grätzel, M.; Mhaisalkar, S.; Sum, T. C. *Nat. Mater.* **2014**, *13* (5), 476.

(7) Zhu, H.; Fu, Y.; Meng, F.; Wu, X.; Gong, Z.; Ding, Q.; Gustafsson, M. V.; Trinh, M. T.; Jin, S.; Zhu, X. *Nat. Mater.* **2015**, *14* (6), 636.
(8) Ren, A.; Wang, H.; Zhang, W.; Wu, J.; Wang, Z.; Penty, R. V.; White, I. H. *Nature Electronics* **2021**, *4* (8), 559−572.
(9) Gandini, M.; Villa, I.; Beretta, M.; Gotti, C.; Imran, M.; Carulli, F.; Fantuzzi, E.; Sassi, M.; Zaffalon, M.; Brofferio, C.; Manna, L.; Beverina, L.; Vedda, A.; Fasoli, M.; Gironi, L.; Brovelli, S. *Nat. Nanotechnol.* **2020**, *15* (6), 462−468.
(10) Liu, Y.; Zaffalon, M. L.; Zito, J.; Cova, F.; Moro, F.; Fanciulli, M.; Zhu, D.; Toso, S.; Xia, Z.; Infante, I.; De Trizio, L.; Brovelli, S.; Manna, L. *Chem. Mater.* **2022**, *34* (19), 8603−8612.
(11) Zaffalon, M. L.; Cova, F.; Liu, M.; Cemmi, A.; Di Sarcina, I.; Rossi, F.; Carulli, F.; Erroi, A.; Rodà, C.; Perego, J.; Comotti, A.; Fasoli, M.; Meinardi, F.; Li, L.; Vedda, A.; Brovelli, S. *Nat. Photonics* **2022**, *16* (12), 860−868.
(12) Wei, M.; de Arquer, F. P. G.; Walters, G.; Yang, Z.; Quan, L. N.; Kim, Y.; Sabatini, R.; Quintero-Bermudez, R.; Gao, L.; Fan, J. Z.; Fan, F.; Gold-Parker, A.; Toney, M. F.; Sargent, E. H. *Nature Energy* **2019**, *4* (3), 197−205.
(13) Zhao, H.; Zhou, Y.; Benetti, D.; Ma, D.; Rosei, F. *Nano Energy* **2017**, *37*, 214−223.
(14) Tan, Z.-K.; Moghaddam, R. S.; Lai, M. L.; Docampo, P.; Higler, R.; Deschler, F.; Price, M.; Sadhanala, A.; Pazos, L. M.; Credgington, D.; et al. *Nat. Nanotechnol.* **2014**, *9* (9), 687.
(15) Pan, J.; Quan, L. N.; Zhao, Y.; Peng, W.; Murali, B.; Sarmah, S. P.; Yuan, M.; Sinatra, L.; Alyami, N. M.; Liu, J.; Yassitepe, E.; Yang, Z.; Voznyy, O.; Comin, R.; Hedhili, M. N.; Mohammed, O. F.; Lu, Z. H.; Kim, D. H.; Sargent, E. H.; Bakr, O. M. *Adv. Mater.* **2016**, *28* (39), 8718−8725.
(16) Xiao, Z.; Kerner, R. A.; Zhao, L.; Tran, N. L.; Lee, K. M.; Koh, T.-W.; Scholes, G. D.; Rand, B. P. *Nat. Photonics* **2017**, *11* (2), 108.
(17) Yang, X.; Zhang, X.; Deng, J.; Chu, Z.; Jiang, Q.; Meng, J.; Wang, P.; Zhang, L.; Yin, Z.; You, J. *Nat. Commun.* **2018**, *9* (1), 570.
(18) Kim, Y. H.; Cho, H.; Heo, J. H.; Kim, T. S.; Myoung, N.; Lee, C. L.; Im, S. H.; Lee, T. W. *Adv. Mater.* **2015**, *27* (7), 1248−1254.
(19) Yuan, M.; Quan, L. N.; Comin, R.; Walters, G.; Sabatini, R.; Voznyy, O.; Hoogland, S.; Zhao, Y.; Beauregard, E. M.; Kanjanaboos, P.; et al. *Nat. Nanotechnol.* **2016**, *11* (10), 872.
(20) Yan, F.; Tan, S. T.; Li, X.; Demir, H. V. *Small* **2019**, *15* (47), 1902079.
(21) Cao, M.; Xu, Y.; Li, P.; Zhong, Q.; Yang, D.; Zhang, Q. *Journal of Materials Chemistry C* **2019**, *7* (46), 14412−14440.
(22) Chin, X. Y.; Cortecchia, D.; Yin, J.; Bruno, A.; Soci, C. *Nat. Commun.* **2015**, *6* (1), 7383.
(23) Kahmann, S.; Shulga, A.; Loi, M. A. *Adv. Funct. Mater.* **2020**, *30* (20), 1904174.
(24) Liu, M.; Wan, Q.; Wang, H.; Carulli, F.; Sun, X.; Zheng, W.; Kong, L.; Zhang, Q.; Zhang, C.; Zhang, Q.; Brovelli, S.; Li, L. *Nat. Photonics* **2021**, *15*, 379.
(25) He, M.; Zhang, Q.; Carulli, F.; Erroi, A.; Wei, W.; Kong, L.; Yuan, C.; Wan, Q.; Liu, M.; Liao, X.; Zhan, W.; Han, L.; Guo, X.; Brovelli, S.; Li, L. *ACS Energy Letters* **2022**, 151−158.
(26) Chiba, T.; Hayashi, Y.; Ebe, H.; Hoshi, K.; Sato, J.; Sato, S.; Pu, Y.-J.; Ohisa, S.; Kido, J. *Nat. Photonics* **2018**, *12* (11), 681−687.
(27) Cao, Y.; Wang, N.; Tian, H.; Guo, J.; Wei, Y.; Chen, H.; Miao, Y.; Zou, W.; Pan, K.; He, Y.; Cao, H.; Ke, Y.; Xu, M.; Wang, Y.; Yang, M.; Du, K.; Fu, Z.; Kong, D.; Dai, D.; Jin, Y.; Li, G.; Li, H.; Peng, Q.; Wang, J.; Huang, W. *Nature* **2018**, *562* (7726), 249−253.
(28) Song, J.; Fang, T.; Li, J.; Xu, L.; Zhang, F.; Han, B.; Shan, Q.; Zeng, H. *Adv. Mater.* **2018**, *30* (50), 1805409.
(29) Xu, W.; Hu, Q.; Bai, S.; Bao, C.; Miao, Y.; Yuan, Z.; Borzda, T.; Barker, A. J.; Tyukalova, E.; Hu, Z.; Kawecki, M.; Wang, H.; Yan, Z.; Liu, X.; Shi, X.; Uvdal, K.; Fahlman, M.; Zhang, W.; Duchamp, M.; Liu, J.-M.; Petrozza, A.; Wang, J.; Liu, L.-M.; Huang, W.; Gao, F. *Nat. Photonics* **2019**, *13* (6), 418−424.
(30) Dong, Y.; Wang, Y.-K.; Yuan, F.; Johnston, A.; Liu, Y.; Ma, D.; Choi, M.-J.; Chen, B.; Chekini, M.; Baek, S.-W.; Sagar, L. K.; Fan, J.; Hou, Y.; Wu, M.; Lee, S.; Sun, B.; Hoogland, S.; Quintero-Bermudez, R.; Ebe, H.; Todorovic, P.; Dinic, F.; Li, P.; Kung, H. T.; Saidaminov, M. I.; Kumacheva, E.; Spiecker, E.; Liao, L.-S.; Voznyy, O.; Lu, Z.-H.; Sargent, E. H. *Nat. Nanotechnol.* **2020**, *15* (8), 668−674.
(31) Dong, Y.; Wang, Y.-K.; Yuan, F.; Johnston, A.; Liu, Y.; Ma, D.; Choi, M.-J.; Chen, B.; Chekini, M.; Baek, S.-W.; Sagar, L. K.; Fan, J.; Hou, Y.; Wu, M.; Lee, S.; Sun, B.; Hoogland, S.; Quintero-Bermudez, R.; Ebe, H.; Todorovic, P.; Dinic, F.; Li, P.; Kung, H. T.; Saidaminov, M. I.; Kumacheva, E.; Spiecker, E.; Liao, L.-S.; Voznyy, O.; Lu, Z.-H.; Sargent, E. H. *Nat. Nano* **2020**, *15*, 668.
(32) Yan, F.; Xing, J.; Xing, G.; Quan, L.; Tan, S. T.; Zhao, J.; Su, R.; Zhang, L.; Chen, S.; Zhao, Y.; et al. *Nano Lett.* **2018**, *18* (5), 3157−3164.
(33) Fakharuddin, A.; Gangishetty, M. K.; Abdi-Jalebi, M.; Chin, S.-H.; bin Mohd Yusoff, A. R.; Congreve, D. N.; Tress, W.; Deschler, F.; Vasilopoulou, M.; Bolink, H. J. *Nature Electronics* **2022**, *5* (4), 203−216.
(34) Yan, F.; Demir, H. V. *Nanoscale* **2019**, *11* (24), 11402−11412.
(35) Song, J.; Li, J.; Li, X.; Xu, L.; Dong, Y.; Zeng, H. *Adv. Mater.* **2015**, *27* (44), 7162−7167.
(36) Liu, F.; Zhang, Y.; Ding, C.; Kobayashi, S.; Izuishi, T.; Nakazawa, N.; Toyoda, T.; Ohta, T.; Hayase, S.; Minemoto, T. *ACS Nano* **2017**, *11* (10), 10373−10383.
(37) Koscher, B. A.; Swabeck, J. K.; Bronstein, N. D.; Alivisatos, A. P. *J. Am. Chem. Soc.* **2017**, *139* (19), 6566−6569.
(38) Nedelcu, G.; Protesescu, L.; Yakunin, S.; Bodnarchuk, M. I.; Grotevent, M. J.; Kovalenko, M. V. *Nano Lett.* **2015**, *15* (8), 5635−5640.
(39) Zhang, Y.; Liu, J.; Wang, Z.; Xue, Y.; Ou, Q.; Polavarapu, L.; Zheng, J.; Qi, X.; Bao, Q. *Chem. Commun.* **2016**, *52* (94), 13637−13655.
(40) Chin, X. Y.; Perumal, A.; Bruno, A.; Yantara, N.; Veldhuis, S. A.; Martínez-Sarti, L.; Chandran, B.; Chirvony, V.; Lo, A. S.-Z.; So, J.; Soci, C.; Grätzel, M.; Bolink, H. J.; Mathews, N.; Mhaisalkar, S. G. *Energy Environ. Sci.* **2018**, *11* (7), 1770−1778.
(41) Zhang, B.; Goldoni, L.; Lambruschini, C.; Moni, L.; Imran, M.; Pianetti, A.; Pinchetti, V.; Brovelli, S.; De Trizio, L.; Manna, L. *Nano Lett.* **2020**, *20* (12), 8847−8853.
(42) Salim, K. M. M.; Hassanabadi, E.; Masi, S.; Gualdrón-Reyes, A. F.; Franckevicius, M.; Devižis, A.; Gulbinas, V.; Fakharuddin, A.; Mora-Seró, I. *ACS Applied Electronic Materials* **2020**, *2* (8), 2525−2534.
(43) Dirin, D. N.; Protesescu, L.; Trummer, D.; Kochetygov, I. V.; Yakunin, S.; Krumeich, F.; Stadie, N. P.; Kovalenko, M. V. *Nano Lett.* **2016**, *16* (9), 5866−5874.
(44) Fang, H.-H.; Protesescu, L.; Balazs, D. M.; Adjokatse, S.; Kovalenko, M. V.; Loi, M. A. *Small* **2017**, *13* (32), 1700673.
(45) Kim, Y.-H.; Kim, S.; Kakekhani, A.; Park, J.; Park, J.; Lee, Y.-H.; Xu, H.; Nagane, S.; Wexler, R. B.; Kim, D.-H.; Jo, S. H.; Martínez-Sarti, L.; Tan, P.; Sadhanala, A.; Park, G.-S.; Kim, Y.-W.; Hu, B.; Bolink, H. J.; Yoo, S.; Friend, R. H.; Rappe, A. M.; Lee, T.-W. *Nat. Photonics* **2021**, *15* (2), 148−155.
(46) Guo, Y.; Apergi, S.; Li, N.; Chen, M.; Yin, C.; Yuan, Z.; Gao, F.; Xie, F.; Brocks, G.; Tao, S.; Zhao, N. *Nat. Commun.* **2021**, *12* (1), 644.
(47) Miao, Y.; Cheng, L.; Zou, W.; Gu, L.; Zhang, J.; Guo, Q.; Peng, Q.; Xu, M.; He, Y.; Zhang, S.; Cao, Y.; Li, R.; Wang, N.; Huang, W.; Wang, J. *Light: Science & Applications* **2020**, *9* (1), 89.
(48) Liu, M.; Wan, Q.; Wang, H.; Carulli, F.; Sun, X.; Zheng, W.; Kong, L.; Zhang, Q.; Zhang, C.; Zhang, Q.; Brovelli, S.; Li, L. *Nat. Photonics* **2021**, *15* (5), 379−385.
(49) Zeng, Q.; Zhang, X.; Bing, Q.; Xiong, Y.; Yang, F.; Liu, H.; Liu, J.-y.; Zhang, H.; Zheng, W.; Rogach, A. L.; Yang, B. *ACS Energy Letters* **2022**, *7* (6), 1963−1970.
(50) Todorović, P.; Ma, D.; Chen, B.; Quintero-Bermudez, R.; Saidaminov, M. I.; Dong, Y.; Lu, Z. H.; Sargent, E. H. *Advanced Optical Materials* **2019**, *7* (24), 1901440.
(51) Shen, X.; Zhang, Y.; Kershaw, S. V.; Li, T.; Wang, C.; Zhang, X.; Wang, W.; Li, D.; Wang, Y.; Lu, M.; Zhang, L.; Sun, C.; Zhao, D.; Qin, G.; Bai, X.; Yu, W. W.; Rogach, A. L. *Nano Lett.* **2019**, *19* (3), 1552−1559.


https://doi.org/10.1021/acsenergylett.2c02802
ACS Energy Lett. 2023, 8, 927−934

(52) Lorenzon, M.; Sortino, L.; Akkerman, Q.; Accornero, S.; Pedrini, J.; Prato, M.; Pinchetti, V.; Meinardi, F.; Manna, L.; Brovelli, S. *Nano Lett.* **2017**, *17* (6), 3844−3853.
(53) Hassan, Y.; Park, J. H.; Crawford, M. L.; Sadhanala, A.; Lee, J.; Sadighian, J. C.; Mosconi, E.; Shivanna, R.; Radicchi, E.; Jeong, M.; Yang, C.; Choi, H.; Park, S. H.; Song, M. H.; De Angelis, F.; Wong, C. Y.; Friend, R. H.; Lee, B. R.; Snaith, H. J. *Nature* **2021**, *591* (7848), 72−77.
(54) Fang, Z.; Chen, W.; Shi, Y.; Zhao, J.; Chu, S.; Zhang, J.; Xiao, Z. *Adv. Funct. Mater.* **2020**, *30* (12), 1909754.
(55) Fakharuddin, A.; Qiu, W.; Croes, G.; Devižis, A.; Gegevičius, R.; Vakhnin, A.; Rolin, C.; Genoe, J.; Gehlhaar, R.; Kadashchuk, A.; Gulbinas, V.; Heremans, P. *Adv. Funct. Mater.* **2019**, *29* (37), 1904101.
(56) Qin, C.; Matsushima, T.; Potscavage, W. J.; Sandanayaka, A. S. D.; Leyden, M. R.; Bencheikh, F.; Goushi, K.; Mathevet, F.; Heinrich, B.; Yumoto, G.; Kanemitsu, Y.; Adachi, C. *Nat. Photonics* **2020**, *14* (2), 70−75.
(57) Lee, S.; Kim, D. B.; Hamilton, I.; Daboczi, M.; Nam, Y. S.; Lee, B. R.; Zhao, B.; Jang, C. H.; Friend, R. H.; Kim, J.-S.; Song, M. H. *Adv. Sci.* **2018**, *5* (11), 1801350.
(58) Ma, D.; Lin, K.; Dong, Y.; Choubisa, H.; Proppe, A. H.; Wu, D.; Wang, Y.-K.; Chen, B.; Li, P.; Fan, J. Z.; Yuan, F.; Johnston, A.; Liu, Y.; Kang, Y.; Lu, Z.-H.; Wei, Z.; Sargent, E. H. *Nature* **2021**, *599* (7886), 594−598.
(59) Jung, Y.-J.; Cho, S.-Y.; Jung, J.-W.; Kim, S.-Y.; Lee, J.-H. *Nano Convergence* **2019**, *6* (1), 26.
(60) Morgenstern, T.; Lampe, C.; Naujoks, T.; Jurow, M.; Liu, Y.; Urban, A. S.; Brütting, W. *J. Lumin.* **2020**, *220*, 116939.
(61) Höfle, S.; Lutz, T.; Egel, A.; Nickel, F.; Kettlitz, S. W.; Gomard, G.; Lemmer, U.; Colsmann, A. *ACS Photonics* **2014**, *1* (10), 968−973.
(62) Zhao, L.; Lee, K. M.; Roh, K.; Khan, S. U. Z.; Rand, B. P. *Adv. Mater.* **2019**, *31* (2), 1805836.
(63) Shi, X.-B.; Liu, Y.; Yuan, Z.; Liu, X.-K.; Miao, Y.; Wang, J.; Lenk, S.; Reineke, S.; Gao, F. *Advanced Optical Materials* **2018**, *6* (17), 1800667.
(64) Zhang, Q.; Zhang, D.; Fu, Y.; Poddar, S.; Shu, L.; Mo, X.; Fan, Z. *Adv. Funct. Mater.* **2020**, *30* (38), 2002570.
(65) Cho, C.; Zhao, B.; Tainter, G. D.; Lee, J.-Y.; Friend, R. H.; Di, D.; Deschler, F.; Greenham, N. C. *Nat. Commun.* **2020**, *11* (1), 611.
(66) Bowman, A. R.; Anaya, M.; Greenham, N. C.; Stranks, S. D. *Phys. Rev. Lett.* **2020**, *125* (6), 067401.
(67) Will, P.-A.; Schmidt, M.; Eckhardt, K.; Wisser, F.; Lenk, S.; Grothe, J.; Kaskel, S.; Reineke, S. *Adv. Funct. Mater.* **2019**, *29* (20), 1901748.
(68) Qu, Y.; Kim, J.; Coburn, C.; Forrest, S. R. *ACS Photonics* **2018**, *5* (6), 2453−2458.
(69) Vandersteegen, P.; Nieto, A.; Van Buggenhout, C.; Verstuyft, S.; Bienstman, P.; Debackere, P.; Neyts, K.; Baets, R. Employing a 2D surface grating to improve light out coupling of a substrate emitting organic LED. *SPIE* **2007**, *6486*, 64860H DOI: 10.1117/12.701344.
(70) Cheng, Y.-H.; Wu, J.-L.; Cheng, C.-H.; Syao, K.-C.; Lee, M.-C. M. *Appl. Phys. Lett.* **2007**, *90* (9), 091102.
(71) Liang, H.; Zhu, R.; Dong, Y.; Wu, S.-T.; Li, J.; Wang, J.; Zhou, J. *Opt. Express* **2015**, *23* (10), 12910−12922.
(72) Slootsky, M.; Forrest, S. R. *Opt. Lett.* **2010**, *35* (7), 1052−1054.
(73) Möller, S.; Forrest, S. R. *J. Appl. Phys.* **2002**, *91* (5), 3324−3327.
(74) Shen, Y.; Cheng, L.-P.; Li, Y.-Q.; Li, W.; Chen, J.-D.; Lee, S.-T.; Tang, J.-X. *Adv. Mater.* **2019**, *31* (24), 1901517.
(75) Kumar, S.; Marcato, T.; Krumeich, F.; Li, Y.-T.; Chiu, Y.-C.; Shih, C.-J. *Nat. Commun.* **2022**, *13* (1), 2106.
(76) Cui, J.; Liu, Y.; Deng, Y.; Lin, C.; Fang, Z.; Xiang, C.; Bai, P.; Du, K.; Zuo, X.; Wen, K.; Gong, S.; He, H.; Ye, Z.; Gao, Y.; Tian, H.; Zhao, B.; Wang, J.; Jin, Y. *Science Advances* **2021**, *7* (41), No. eabg8458.
(77) Zhang, Q.; Tavakoli, M. M.; Gu, L.; Zhang, D.; Tang, L.; Gao, Y.; Guo, J.; Lin, Y.; Leung, S.-F.; Poddar, S.; Fu, Y.; Fan, Z. *Nat. Commun.* **2019**, *10* (1), 727.
(78) Alias, M. S.; Dursun, I.; Saidaminov, M. I.; Diallo, E. M.; Mishra, P.; Ng, T. K.; Bakr, O. M.; Ooi, B. S. *Opt. Express* **2016**, *24* (15), 16586−16594.
(79) Lin, J.; Dai, X.; Liang, X.; Chen, D.; Zheng, X.; Li, Y.; Deng, Y.; Du, H.; Ye, Y.; Chen, D.; Lin, C.; Ma, L.; Bao, Q.; Zhang, H.; Wang, L.; Peng, X.; Jin, Y. *Adv. Funct. Mater.* **2020**, *30* (5), 1907265.
(80) Lee, S.; Kim, D. B.; Hamilton, I.; Daboczi, M.; Nam, Y. S.; Lee, B. R.; Zhao, B.; Jang, C. H.; Friend, R. H.; Kim, J.-S.; Song, M. H. *Advanced Science* **2018**, *5* (11), 1801350.
(81) Shi, Z.; Li, Y.; Zhang, Y.; Chen, Y.; Li, X.; Wu, D.; Xu, T.; Shan, C.; Du, G. *Nano Lett.* **2017**, *17* (1), 313−321.
(82) Caruge, J. M.; Halpert, J. E.; Wood, V.; Bulović, V.; Bawendi, M. G. *Nat. Photonics* **2008**, *2* (4), 247−250.
(83) Bush, K. A.; Palmstrom, A. F.; Yu, Z. J.; Boccard, M.; Cheacharoen, R.; Mailoa, J. P.; McMeekin, D. P.; Hoye, R. L. Z.; Bailie, C. D.; Leijtens, T.; Peters, I. M.; Minichetti, M. C.; Rolston, N.; Prasanna, R.; Sofia, S.; Harwood, D.; Ma, W.; Moghadam, F.; Snaith, H. J.; Buonassisi, T.; Holman, Z. C.; Bent, S. F.; McGehee, M. D. *Nature Energy* **2017**, *2* (4), 17009.
(84) Chen, W.; Wu, Y.; Yue, Y.; Liu, J.; Zhang, W.; Yang, X.; Chen, H.; Bi, E.; Ashraful, I.; Grätzel, M.; Han, L. *Science* **2015**, *350* (6263), 944.
(85) Seo, S.; Park, I. J.; Kim, M.; Lee, S.; Bae, C.; Jung, H. S.; Park, N.-G.; Kim, J. Y.; Shin, H. *Nanoscale* **2016**, *8* (22), 11403−11412.
(86) Traore, B.; Pedesseau, L.; Blancon, J.-C.; Tretiak, S.; Mohite, A. D.; Even, J.; Katan, C.; Kepenekian, M. *ACS Appl. Mater. Interfaces* **2020**, *12* (5), 6633−6640.
(87) Tsai, H.; Asadpour, R.; Blancon, J.-C.; Stoumpos, C. C.; Durand, O.; Strzalka, J. W.; Chen, B.; Verduzco, R.; Ajayan, P. M.; Tretiak, S.; Even, J.; Alam, M. A.; Kanatzidis, M. G.; Nie, W.; Mohite, A. D. *Science* **2018**, *360* (6384), 67.
(88) Song, J.; Li, J.; Xu, L.; Li, J.; Zhang, F.; Han, B.; Shan, Q.; Zeng, H. *Adv. Mater.* **2018**, *30* (30), 1800764.
(89) Li, Z.; Chen, Z.; Yang, Y.; Xue, Q.; Yip, H.-L.; Cao, Y. *Nat. Commun.* **2019**, *10* (1), 1027.
(90) Rodà, C.; Fasoli, M.; Zaffalon, M. L.; Cova, F.; Pinchetti, V.; Shamsi, J.; Abdelhady, A. L.; Imran, M.; Meinardi, F.; Manna, L.; Vedda, A.; Brovelli, S. *Adv. Funct. Mater.* **2021**, *31* (43), 2104879.
(91) Ohta, N.; Robertson, A. R. CIE Standard Colorimetric System. In *Colorimetry*; Kriss, M. A., Ed.; Wiley, 2005; pp 63−114.


https://doi.org/10.1021/acsenergylett.2c02802
*ACS Energy Lett.* 2023, 8, 927−934